Available online at www.sciencedirect.com
SCIENCE DIRECT®
Journal of Solid State Chemistry 173 (2003) 137–147
JOURNAL OF SOLID STATE CHEMISTRY
http://elsevier.com/locate/jssc

Reinvestigation of the GaMn structure and theoretical studies of its electronic and magnetic properties

Olivier Gourdon and Gordon J. Miller*

Department of Chemistry and Ames Laboratory, US Department of Energy, Iowa State University, Ames, IA 50011-3111, USA

Received 30 April 2002; received in revised form 23 July 2002; accepted 27 August 2002

Abstract

The crystal structure of the binary gallide compound GaMn is reinvestigated using X-ray diffraction. The structure is quite different from that proposed previously. Although GaMn is reported to crystallize with the Al_8Cr_5 structure type, space group $R3m$, we found that the centrosymmetric space group $R\bar{3}m$, with $a = 12.605(2)$ Å and $c = 8.0424(11)$ Å, was more accurate. Moreover, the atomic positions and the atomic displacement parameters, which are missing in the previous study, are now refined. Thereafter, band structure calculations have been performed using the TB-LMTO-ASA method to understand the electronic and magnetic properties of this compound. Analyses from the band structure, the density of states and the magnetic moments obtained using spin-polarized calculations show the stability of two different magnetic models relative to the nonmagnetic one.

Keywords: Intermetallic compounds; Gallium; Manganese; Ab initio band structure calculations; Spin polarization; Magnetism

1. Introduction

In the phase diagram of the binary system Ga–Mn, numerous phases have been reported, viz., Ga_2Mn_3 [1], Ga_3Mn_7 [2], Ga_3Mn [3], Ga_5Mn [4], Ga_5Mn_2 [5], Ga_5Mn_8 [5], $GaMn_3$ [6,7] and GaMn [3]. Many of the known compounds can be considered as crystalline approximants to quasicrystals that consist of connected icosahedra and dodecahedra. However, to our knowledge, GaMn [3] has not been studied structurally since the 1960s, and is limited to just unit-cell parameters but no atomic parameters or structural details. According to Refs [3,5], GaMn adopts the Al_8Cr_5 structure type with a superstructure along the *c*-axis. Besides these structural considerations, Mn or Cr alloys with group 13 metals are of interest due to their remarkable spin-density-wave (SDW) magnetic behavior [8]. Progress of thin-film fabrication techniques has made it possible to grow ferromagnetic, metallic GaMn films with the CuAu structure type (δ-GaMn) on semiconductor substrates [9]. Some theoretical studies have been performed to understand this ferromagnetic behavior [10,11].

These different points of interest motivated us to reinvestigate the crystal structure as well as the electronic and magnetic structure of GaMn. Using X-ray diffraction the atomic structure of GaMn has been definitively solved and found to be quite different from that proposed previously [3]. Thereafter, band structure calculations have been performed using the TB-LMTO-ASA method to understand the electronic and possible magnetic properties of this compound. Spin polarized calculations are necessary to discuss the magnetic behavior of this structure. Analyses from the band structure, the density of states and the calculated magnetic moments show that two different magnetic models are more stable than the paramagnetic one. These two models will be compared and a schematic magnetic model for GaMn will be proposed.

2. Experimental

2.1. Synthesis and analyses

GaMn samples were obtained from a mixture of the elements in the same molar ratio (Ga shot (99.999%, Aldrich) and Mn powder (99.9%, Alfa)). The Mn

*Corresponding author. Fax: +1-515-294-0105.
E-mail address: gmiller@iastate.edu (G.J. Miller).

0022-4596/03/$ - see front matter © 2002 Elsevier Science (USA). All rights reserved.
PII: S0022-4596(02)00031-2

powder was treated by first heating it with an arc welder furnace to remove adventitious oxygen. The mixture of treated manganese and gallium was placed in a sealed, evacuated silica tube at 1023 K for 4 days. After slow cooling (30 h) to 723 K, the closed furnace was turned off and cooled naturally to room temperature. Small plates with a metallic luster were found inside the batch. Powder diffraction and single-crystal analysis have been performed to characterize the sample. At least three phases were identified: $GaMn_3$, Ga_5Mn_8 and GaMn. The growth of a pure GaMn sample is difficult according to the characteristics of the Ga–Mn binary phase diagram [12], because, various phases coexist and the growth from the liquidus with 1:1 composition implies first the formation of other binary compounds. These crystals are stable to exposure to air and water. Dilute acid is helpful to eliminate the Ga excess from the flux without damaging the crystal, whereas concentrated acid dissolves the flux and the crystals. Moreover, several attempts to quench the liquid did not procedure pure, single-phase product.

Some single crystals, which were recognized by X-ray diffraction as GaMn single crystals, were examined by electron microprobe (JEOL 840A) and found to be free of other elements. Analysis by energy-dispersive X-ray spectroscopy gave the average chemical composition $Ga_{0.52(2)}Mn_{0.48(2)}$. To obtain the quantitative values, GaAs and Mn were used as standards.

2.2. Structure determination

X-ray diffraction studies were carried out with a single crystal of approximately $0.1 \times 0.1 \times 0.01\,mm^3$ in size on a P4 Siemens X-ray diffractometer using Mo$K\alpha$ radiation ($\lambda = 0.71073$ Å). Reflections were adjusted for Lorentz polarization and subsequently corrected for absorption via a Gaussian analytical method (the crystal shape and dimensions were optimized with the STOE *X-shape* program [13] on the basis of equivalent reflections). Thereafter, the set of reflections was subsequently merged according to the $\bar{3}m$ point group ($R_{int} = 0.045$ at a 2σ level). A quick analysis of the extinction rules space groups indicated that $R\bar{3}m$ or $R3m$ are possible. The structure was refined (F^2, all reflections included) using the JANA2000 program [14] with the atomic positions of the Al_8Cr_5 structure type as proposed by Schubert et al. [3] and with the noncentrosymmetric space group $R3m$. As a starting point, the nine atomic sites were considered to be Ga sites with an isotropic thermal displacement due to the fact that the atomic positions for GaMn ("Al_8Cr_5" structure type) are not listed in the literature. After a few cycles, the R-value converged quickly to a value close to 9%. Moreover, the thermal displacement of five sites became too large and could be explained by the fact that these sites are occupied by Mn atoms. By placing Mn atoms at these sites and using anisotropic thermal displacements, the R-value converged to the final solution of $R = 3.45\%$ for 52 parameters. However, a quick look at the refinement shows some correlations between the atomic positions and the thermal displacement parameters at two Mn sites and also between two Ga sites, which suggested that a symmetry element is missing. Indeed, by shifting

Table 1
Crystallographic data for GaMn

(1) *Physical, crystallographic, and analytical data*	
Formula	$Ga_{13}Mn_{13}$
Crystal color	Dark brown
Molecular weight (g.mol^{-1})	1620.55
Crystal system	Trigonal
Space group	$R\bar{3}m$
Temperature (K)	293
Cell parameters (from 26 2θ positions obtained from the P4 measurement)	
a (Å)	12.605(2)
c (Å)	8.0424(11)
V (Å^3)	1106.6(3)
Z	3
Density (calc., g cm^{-3})	7.243
Crystal description	Plate
Crystal size (mm^3)	$\sim 0.1 \times 0.1 \times 0.01$
(2) *Data collection*	Siemens P4
Monochromator	Oriented graphite (0 0 2)
Radiation	Mo$KL_{2,3}$ ($\lambda = 0.71073$ Å)
Scan mode	$\omega/2\theta$
No. of measured reflections	1065
hkl range	$-13 < h < 0$ $0 < k < 15$ $-9 < l < 9$
$\sin(\theta)/\lambda$ range	0–0.8
No. of standard reflections	3
Frequency of standard reflections (s)	3600
(3) *Data reduction*	Siemens P4
Linear absorption coeff. (cm^{-1})	336.71
Absorption correction	Analytical
T_{min}/T_{max}	0.10/0.23
Number of reflections	1065
No. of independent reflections	280
Criterions for observed reflections	$I > 3\sigma(I)$
R_{int} (obs)	4.50
No. of observed reflections	469
(4) *Refinement*	
Refinement	F^2
$F(000)$	2184
No. of reflections used in the refinement	247
R (%)[a]	3.48
R_w (%)[a]	7.72
S	1.98
No. of refined parameters	29
Weighting scheme	$w = 1/(\sigma F_o)^2 + (0.01 \times \lvert F_o \rvert)^2)$
Difference Fourier residues	[−2.68, +2.65] e$^-$/Å^3

[a] $R = \sum ||F_o| - |F_c|| / \sum |F_o|$. $R_w = [\sum w(|F_o| - |F_c|)^2 / \sum w|F_o|^2]^{1/2}$.

all the atomic positions along the z-axis (according to the atomic positions of the Al_8Cr_5), an inversion center could be identified in the description of the structure. So, the centrosymmetric space group $R\bar{3}m$ was finally chosen for the description, which reduced the number of parameters and gave the same R-value. Moreover, the correlations vanish. Ga and Mn have close X-ray scattering factors and mixed site occupancies are commonly observed in other Ga_xMn_y binary compounds except in the three most gallium-rich compounds. Consequently, some tests were attempted to check this possibility, but we did not find this in our case. For each test, starting the refinement with mixed occupancies we converge to full occupancies of Ga or Mn. Two other crystals from the same preparation sample were checked and confirmed Ga or Mn full occupancies in the particular atomic sites. It may be possible that other preparations close to this stoichiometry could give the same structure with mixed occupancies between Ga and Mn on some sites.

Schubert et al. [3,5] suspected that a superstructure along the c-axis ($c = 2c'$) is present. To look for this possible superstructure, the intensities of possible ($hkl/2$) reflections were checked, but none were present, and so no superstructure was found. The main crystallographic data, the atomic coordinates, anisotropic displacement parameters and important interatomic distances are listed in Tables 1–4.

Table 2
Fractional atomic coordinates and equivalent isotropic displacement parameters[a] (Å^2) for GaMn

	x	y	z	B_{eq}
Ga1	0	0	0	0.85(7)
Mn2	0	0	1/2	0.66(6)
Ga3	0.2324(13)	0.11617	0.5757(2)	1.15(4)
Mn4	0.23659(16)	0.11830	0.9295(2)	0.68(5)
Mn5	−0.14653(16)	−0.07326	0.7510(2)	0.71(5)
Ga6	0.62154(11)	0.62154	1/2	0.97(4)

[a] $B_{eq} = 8\pi^2/3 \sum_i \sum_j U_{ij} a_i^* a_j^* \mathbf{a}_i \mathbf{a}_j$.

3. Structural discussion

The GaMn structure is related to the Al_8Cr_5 structure type but adopts a centrosymmetric space group. This structure can be considered as one of the simplest approximants of quasicrystals such as Al_3Mn [15–17], $Al_{60}Mn_{11}Ni_4$ [18] or $Ga_{137}Mn_{123}$ [19]. Therefore, we develop this structure from the viewpoint of condensed clusters.

Surrounding each lattice point, which is occupied by a Ga atom, is a nearly regular icosahedron of Mn atoms at a distance of ca. 2.6 Å, shown in Fig. 1a. This feature is common for gallides or aluminides of transition metals [2,3,15,16,17]: the icosahedron is built of metal atoms around the Ga or Al site. The second shell, illustrated in Fig. 1b, is a pentagonal dodecahedron

Table 3
Anisotropic displacement parameters U_{ij}[a] (Å^2) for GaMn

	U_{11}	U_{22}	U_{33}	U_{12}	U_{13}	U_{23}
Ga1	0.0087(10)	0.0087	0.0141(16)	0.0043(5)	0	0
Mn2	0.0056(13)	0.0056	0.011(2)	0.0028(7)	0	0
Ga3	0.0090(7)	0.0158(8)	0.0164(7)	0.045(4)	0.0005(5)	0.0003
Mn4	0.0078(9)	0.0063(7)	0.0119(9)	0.0039(4)	0.0007(7)	0.0004
Mn5	0.0095(10)	0.0065(7)	0.0116(10)	0.0048(5)	0.0019(8)	0.0009
Ga6	0.0113(5)	0.0113(6)	0.0163(7)	0.0074(6)	0.0012(3)	−0.0012

[a] The anisotropic displacement factor exponent takes the form $(-2\pi^2 \sum_i \sum_j U_{ij} a_i^* a_j^* h_i h_j)$.

Table 4
Main interatomic distances (Å) in GaMn

Icosahedral site		Dodecahedral site			
Ga1–Mn3	2.6441(17) × 6	Ga1–Mn2	4.0212 × 2	Mn2–Mn4	2.576 (2) × 6
Ga1–Mn4	2.5626(17) × 6	Ga1–Ga3	4.2515 (14) × 6		
		Ga1–Ga6	4.1695 (15) × 12		
Mn3–Mn3	2.820 (2) × 6				
Mn3–Mn4	2.675 (2) × 12	Ga3–Mn2	2.609 (2) × 6		
Mn3–Mn4	2.750 (2) × 6	Ga6–Ga6	2.8560 (5) × 6		
Mn4–Mn4	2.771 (2) × 6	Ga6–Ga6	3.0643 (13) × 6		
		Ga3–Ga6	3.218 (2) × 12		

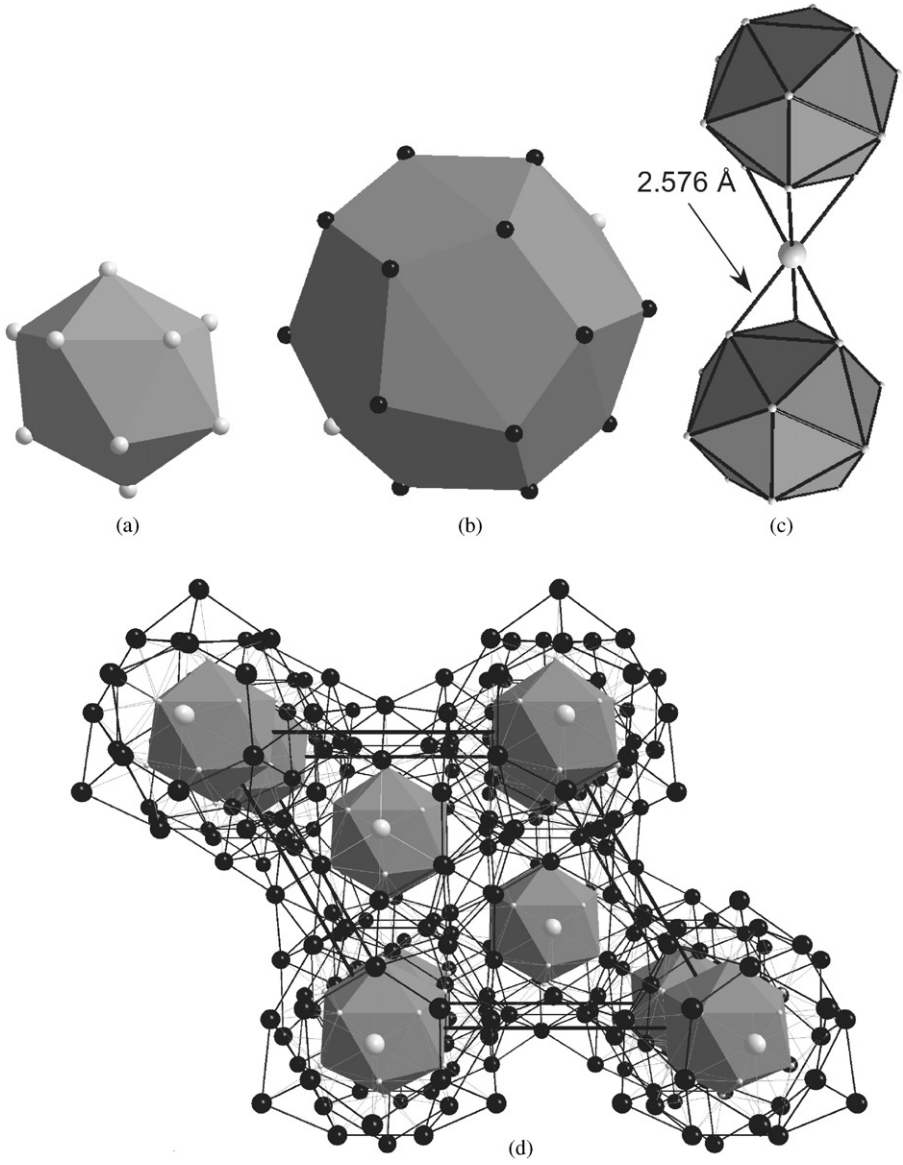

Fig. 1. Illustration of the some clusters in the GaMn structure: (a) icosahedra of Mn around a Ga site; (b) pentagon–dodecahedra of 18 Ga sites and two Mn sites; (c) connection between two icosahedra via the Mn site on the pentagon–dodecahedra; (d) unit cell along the *c*-axis showing the icosahedra mostly surrounded by Ga atoms. The gray and black spheres represent the Mn atoms and Ga atoms, respectively.

composed of 18 Ga atoms (in black) and two Mn atoms (in light gray) at ca. 4.2 Å from the central Ga atom. The icosahedron and the dodecahedron are the two dual polyhedra building up this structure. However, we should note that the shortest distances (2.576 Å) in the structure are between Mn atoms of the icosahedron and Mn atoms of the dodecahedron (Fig. 1c and Table 4). These Mn–Mn bonds between two clusters create two tetrahedra as shown in Fig. 1c. In Fig. 1d we illustrate the arrangement of the icosahedral sites in the unit cell surrounded mostly by Ga atoms of the dodecahedral clusters.

3.1. Cluster description

Recently, a new binary Ga–Mn compound, $Ga_{137}Mn_{123}$, has been reported with a new structure type [19]. After the discovery of this new compound, Boström and his coworkers have discussed the connection and the extension of such clusters (icosahedra and dodecahedra) in different approximants to decagonal quasicrystals [20]. It appears to us that the GaMn structure, which was absent in this discussion, can contribute to this description. Indeed, in Fig. 1d we have seen that the icosahedra are not directly connected to

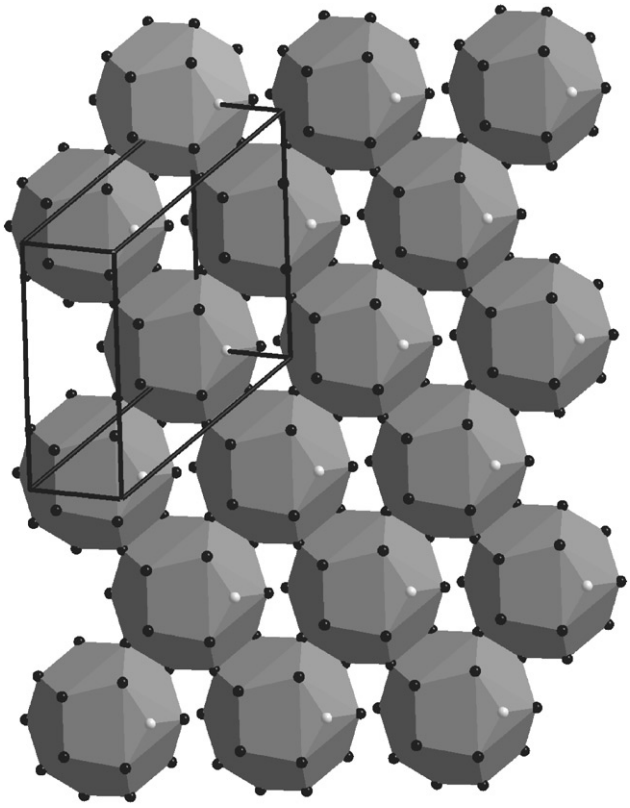

Fig. 2. Plane of pentagon–dodecahedra connected by Ga–Ga edges.

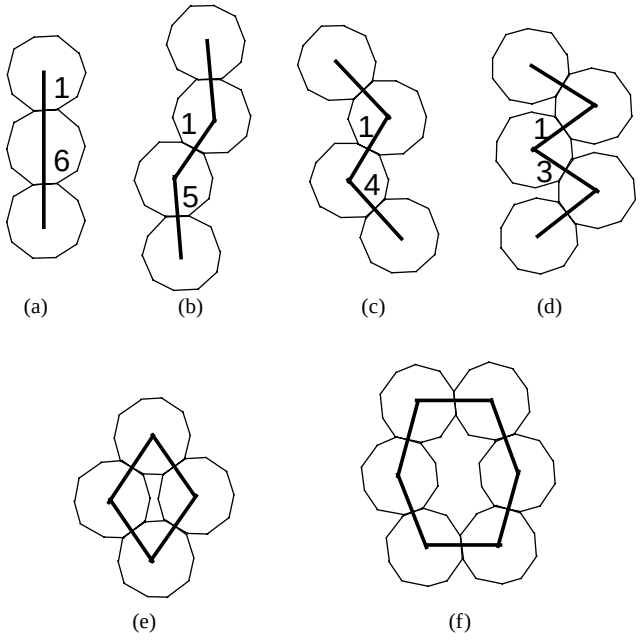

Fig. 3. Hypothetical connections between pentagon–dodecahedra in quasicrystal approximants as referenced by Boström et al. [19]. The nomenclature is derived from that used for cyclic organic compounds (numbering of the edges). (a) 1–6 strand found in $Al_{60}Mn_{11}Ni_4$ [18], (b) 1–5 strand found in Al_3Mn [14–16], (c) 1–4 strand, (d) 1–3 strand, (e) four wheel clusters, (f) six wheel clusters found in $Ga_{137}Mn_{124}$ [19]. (c), (d) and (e) Motifs are found in GaMn.

each other. However, this is not the case for the dodecahedra, which share common Ga–Ga edges creating quasiinfinite planes parallel with (001) as shown in Fig. 2.

Figs. 3a–f present schematically the different possible connections between the dodecahedra as Boström and his coworkers have already suggested. Only the motifs in Figs. 3a, b and f have been observed, respectively, in $Al_{60}Mn_{11}Ni_4$, Al_3Mn and $Ga_{137}Mn_{123}$. However, in the plane of dodecahedra for GaMn shown in Fig. 2, we can find all of them, like the diamond motif (Fig. 3e).

3.2. Close packing description

The GaMn structure can be described as a 2D packing of edge-sharing dodecahedra with diamond motifs. These planes of dodecahedra stack according to a hexagonally close packed motif as shown in Figs. 4a and b (A–B–A–B–⋯). According to Fig. 4c, these planes are connected to each other by a Ga–Ga edge and by the Mn atom on the other dodecahedron.

One of the interests of this structure is the icosahedral cluster of Mn. Due to the difficulty to synthesize a pure sample of this compound; no magnetic measurements have been performed. However, icosahedral clusters composed of magnetic elements like Mn could show some degree of magnetic frustration and potentially interesting magnetic phenomena. Moreover, these icosahedra are not isolated and, from the point of view of magnetism, the Mn sites in the dodecahedra connect two icosahedra along the *c*-axis. Therefore, the electronic and magnetic structure of GaMn could be quite interesting.

4. Electronic structure calculations

Band structure calculations have been performed to understand the electronic and possible magnetic structure of GaMn. As stated previously, GaMn can adopt the CuAu structure type in thin films by a low-temperature synthesis route. Some previous calculations have been done on GaMn with this CuAu structure type [10,11]. Although our structure is totally different and more elaborate than this structure type, these results could be compared to ours. Using spin-polarized calculations, two different magnetic models (FM1 and FM2) have been found to be more stable than the paramagnetic one (PM) using the centrosymmetric space group $R\bar{3}m$. Other calculated models with the noncentrosymmetric space group $R3m$ have been attempted. However, they all converge to either the FM1 or FM2 model and no other magnetic models have been found from our computational efforts.

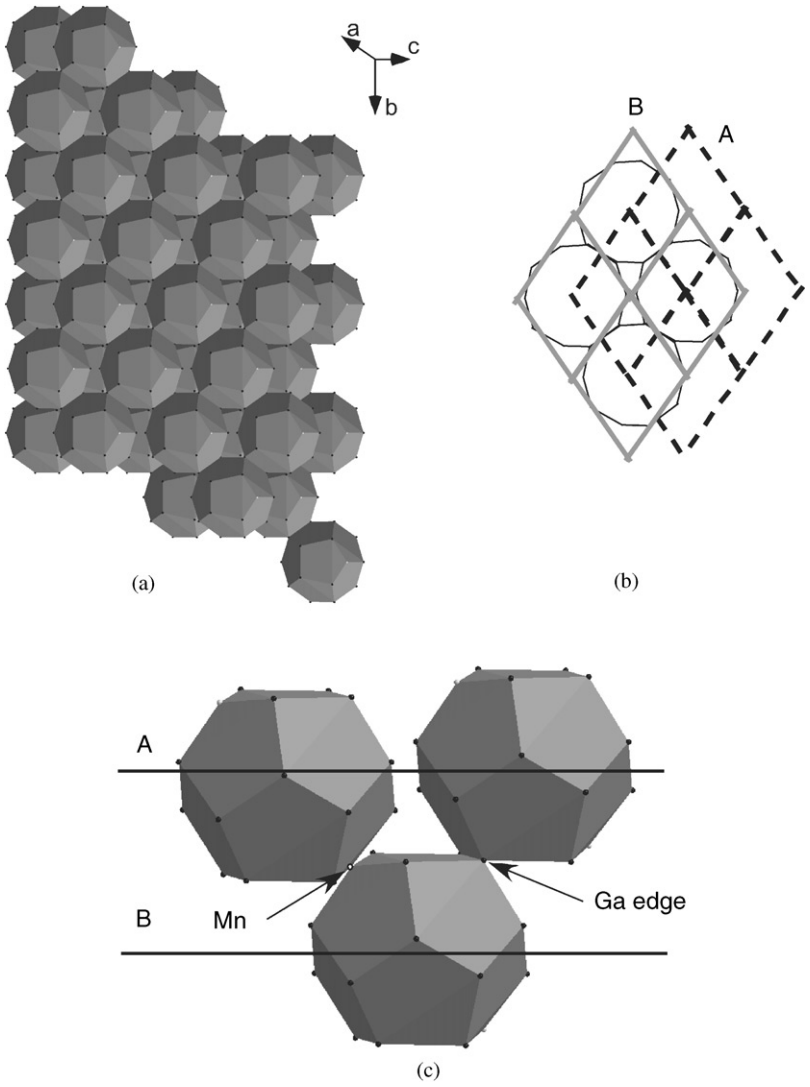

Fig. 4. (a) Perpendicular view and (b) partial schematic view showing the hexagonal close packing (A–B–A–B···) between two planes of pentagon–dodecahedra. (c) View of two dodecahedra of the A plane and one pentagon-dodecahedron of the B plane showing the connection between them with one Ga–Ga edge and one Mn site.

4.1. Computational details

TB-LMTO electronic band structure calculations were carried out for GaMn in the atomic sphere approximation using the LMTO47 program [21]. Exchange and correlation were treated in a local spin density approximation [22]. All relativistic effects except spin–orbit coupling were taken into account using a scalar relativistic approximation [23].

In the atomic sphere approximation, space is filled with small overlapping Wigner–Seitz (WS) atomic spheres. The symmetry of the potential is considered spherical inside each WS sphere, and a combined correction is used to take into account the overlapping part [24]. The radii of the WS spheres were obtained by requiring that the overlapping potential be the best possible approximation to the full potential, and were determined by an automatic procedure described in Ref. [24]. This overlap should not be too large because the error in the kinetic energy introduced by the combined correction is proportional to the fourth power of the relative sphere overlap. Interatomic space was filled with one interstitial sphere since the structure of the compound under examination is not densely packed. The optimal position and radius (r_{ES}) of this "empty sphere" (ES) was determined according to the method described in Ref. [24]. The WS radius of Mn and Ga atoms are nearly equal ($1.47\,\text{Å} < r_{Mn} < 1.48\,\text{Å}$ and $1.45\,\text{Å} < r_{Ga} < 1.46\,\text{Å}$) while the empty sphere has a radius of 0.78 Å is located on the pentagonal faces of the dodecahedra.

The basis set included Ga 4*s*, 4*p*, and 4*d* orbitals and Mn 4*s*, 4*p*, and 3*d* orbitals. For the ES only *s* and *p* orbitals are used. The Ga 4*d* orbital and the ES *p* orbital

were treated by the Löwdin downfolding technique [21]. The **k**-space integrations were performed by the tetrahedron method [25]. The self-consistent charge density was obtained using 32 irreducible **k**-points in the Brillouin zone for the rhombohedral cell. The contribution of the nonspherical part of the charge density to the potential was neglected. Both nonspin-polarized and spin-polarized calculations were performed. The choice of the Fermi level as energy reference has been made.

4.2. Paramagnetic GaMn

In Fig. 5 the total density of states (TDOS) and different partial densities of states (PDOS) for the nonspin-polarized calculations on the GaMn structure are presented (PM). The PDOS of the Mn 4*d* orbitals are presented in Figs. 5b (Mn from the icosahedral sites (ico)) and c (Mn from the dodecahedral sites (dodeca)), whereas the Ga contribution is presented in Fig. 5d, which is essentially from the 4*p* orbitals. The TDOS (Fig. 5a) around the Fermi level corresponds mostly to the Mn 3*d* orbitals. The profile of the TDOS is close to the PDOS for the Mn 3*d* (ico) (Fig. 5b), which suggests that the icosahedra dominate the electronic properties.

The shape of the TDOS in the vicinity of the Fermi level corresponds mostly to two broad peaks: one centered at −2 eV and the second one centered on the Fermi level. The Ga 4*p* PDOS is relatively flat with the highest density around −2 eV. So, a small interaction is expected between the Ga 4*p* orbitals and Mn 3*d* orbitals. The Mn orbitals from the icosahedral sites and the dodecahedral sites have been plotted separately to show the slight difference in the PDOS due to the local environment. The environment of the Mn from the dodecahedral sites, presented in Fig. 1c, is trigonal antiprismatic with six short Mn–Mn distances (2.576 Å). Consequently, the two DOS regions indicate separate Mn–Mn bonding states and Mn–Mn antibonding states, which are also illustrated by the crystal overlap Hamilton population (COHP [26]) curve in Fig. 6a. For the Mn atoms in the icosahedra, various Mn–Mn distances are observed from 2.675 to 2.820 Å. Consequently, the Mn valence orbitals are split by ca. 2 eV, whereas some Mn–Mn interactions for larger distances are observed around −1 eV (Fig. 6b). Integration of the Mn 3*d* PDOS shows that approximately 60%

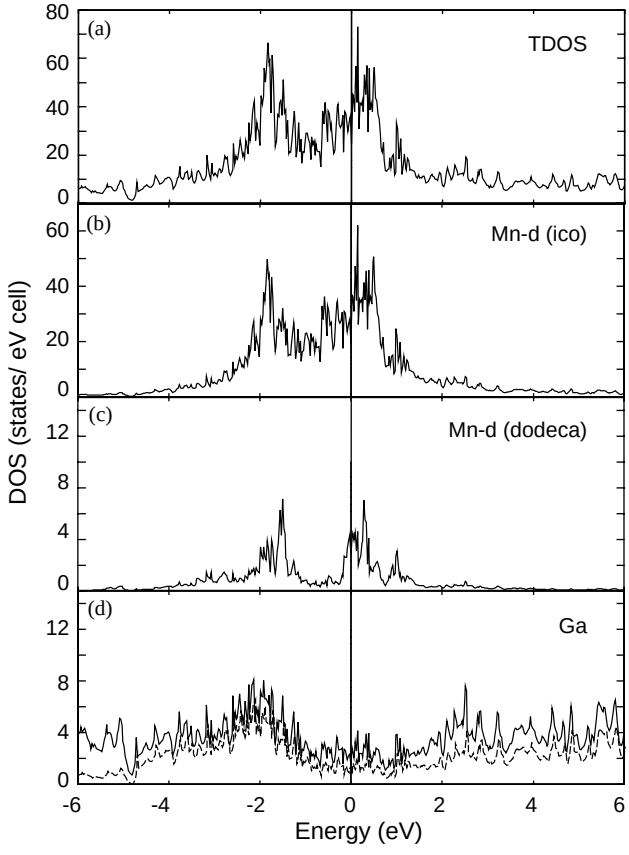

Fig. 5. (a) TDOS and different PDOS for the paramagnetic calculation for GaMn, (b) Mn-*d* PDOS from the icosahedral sites, (c) Mn-*d* PDOS from the pentagon–dodecahedra and (d) Ga PDOS (in dashed line is represented only the Ga-*p* contribution). The Fermi level corresponds to the energy reference.

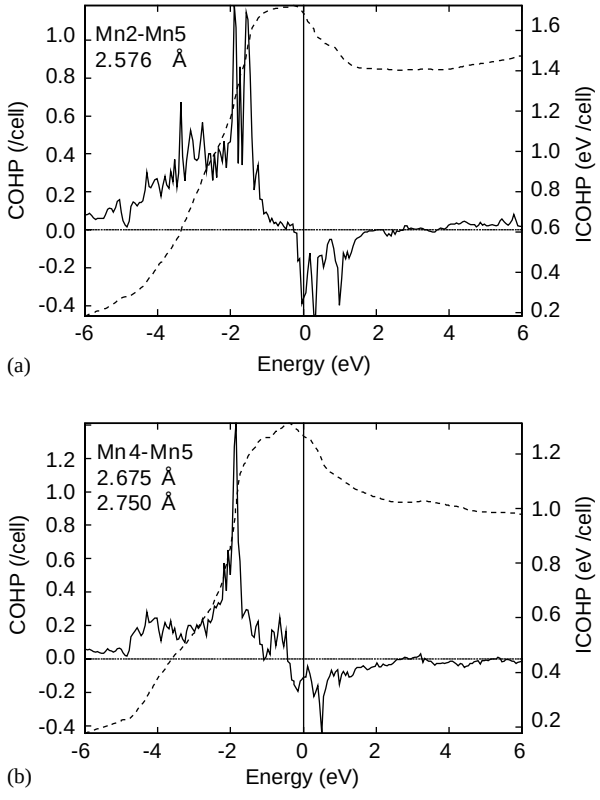

Fig. 6. COHP and integrated COHP (ICOHP) in GaMn for (a) Mn–Mn short distance interactions (between the icosahedral site and the dodecahedral site) and (b) Mn–Mn longer distance interactions (in the icosahedral site).

of the 3*d* states are occupied. Therefore, the last state populated is Mn–Mn antibonding as shown in Fig. 6.

To summarize, calculations without spin polarization show that the DOS at the Fermi level is very high (around 40 states/eV/cell) and these states have Mn–Mn antibonding character (Fig. 6). Dronskowski et al. have already shown that a driving force for ferromagnetism lies in the antibonding character of the states around the Fermi level [27]. Consequently, according to the Stoner criteria [28] and considering the results of band structure calculations performed on ferromagnetic δ-GaMn [10,11], magnetic properties are expected for GaMn and spin-polarized calculations should be performed to understand its electronic structure.

4.3. Spin polarized calculations on GaMn

Since there are no experimental magnetic data available for GaMn, the magnetic calculations that have been carried out are based upon hypothetical magnetic structures. Different initial magnetic models were attempted that retained the threefold symmetry axis, but only two models converged (FM1 and FM2), both of which are centrosymmetric in the potential.

Considering only the Mn sites, which dominate the magnetic behavior, the structure could be easily described as a 1-D magnetic compound. Indeed, along the *c*-axis we observe a regular succession of icosahedra and isolated Mn atoms bridging these icosahedra. The FM1 and FM2 models correspond to two different Mn–Mn coupling arrangements. In the FM1 model the Mn–Mn couplings in the icosahedra are ferromagnetic whereas the Mn–Mn coupling between the icosahedra and the bridging Mn (dodeca) atom is antiferromagnetic (AFM). In the FM2 model, these coupling are opposite. Indeed, the Mn–Mn couplings in the icosahedra are mostly AFM whereas the Mn–Mn coupling between the icosahedra and the bridging Mn (dodeca) atom is ferromagnetic. Let us describe the calculated results for both models.

4.3.1. The FM1 model

According to the results listed in Table 5, FM1 is approximately 1.69 eV more stable (per unit cell) than the paramagnetic model with a global magnetic moment of 25.243 μ_B/cell. Fig. 7 illustrates the TDOS and

Table 5
Results of spin-polarized band structure calculations for the FM1 and FM2 models for GaMn

	FM1	FM2
Ga1 (μ_B)	−0.085	−0.039
Mn2 (μ_B)	−1.979	1.837
Ga3 (μ_B)	−0.048	0.030
Mn4 (μ_B)	2.096	−1.968
Mn5 (μ_B)	2.576	2.352
Ga6 (μ_B)	−0.064	0.053
Total (μ_B/cell)	25.243	4.641
ΔE (eV/cell) (relative to the paramagnetic calculation)	−1.69	−1.45

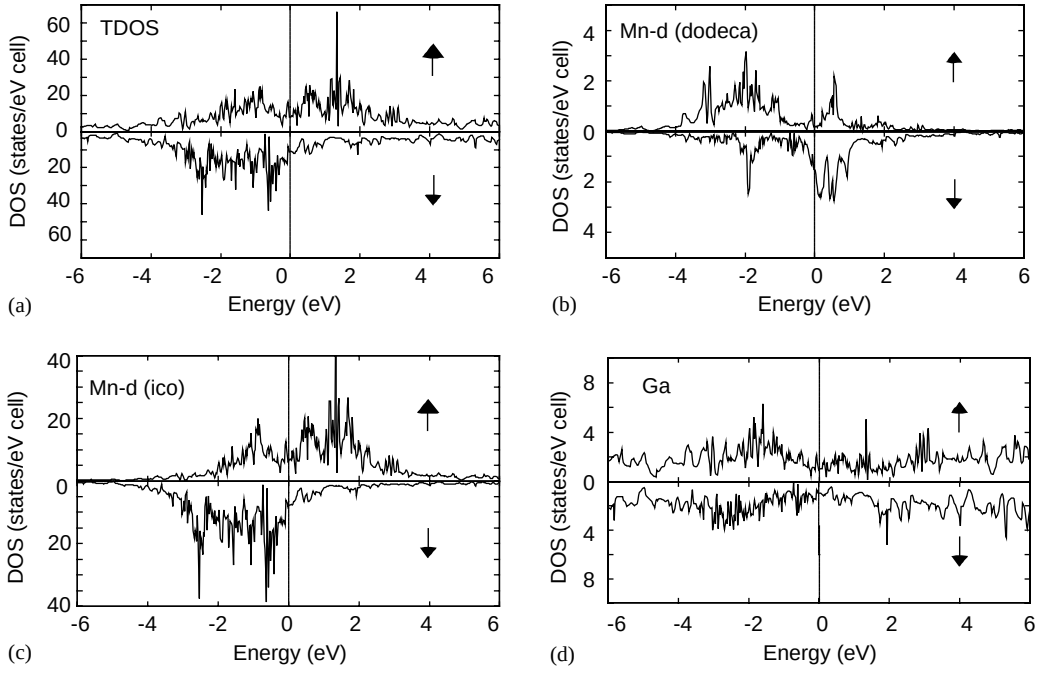

Fig. 7. (a) TDOS and different PDOS for the spin-polarized calculation for GaMn (model FM1), (b) Mn-*d* PDOS from the icosahedral sites, (c) Mn-*d* PDOS from the dodecahedral sites and (d) Ga PDOS.

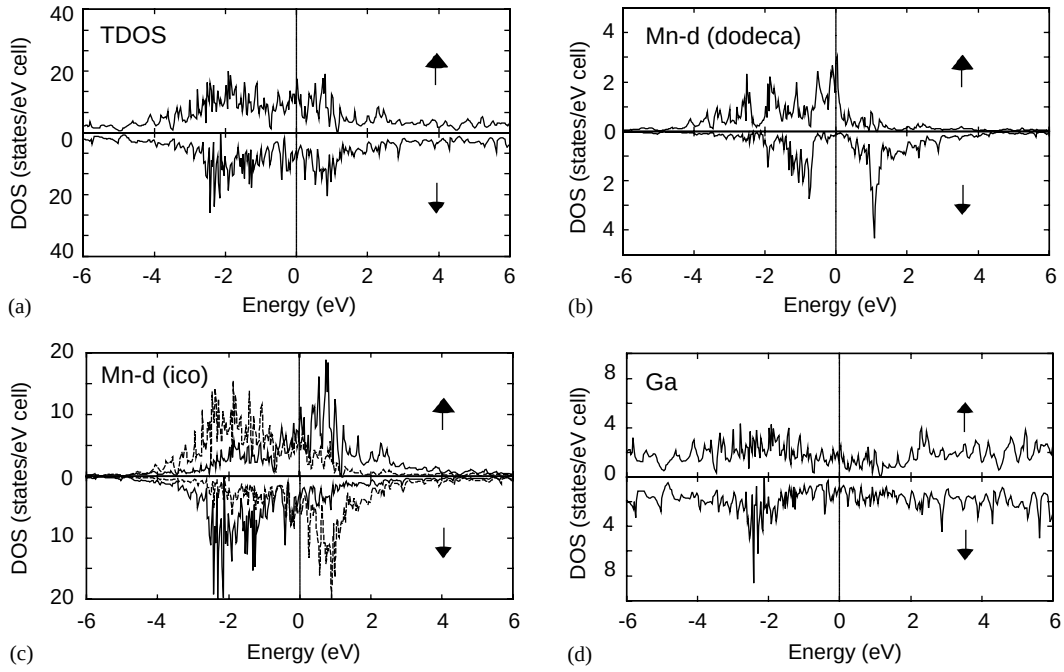

Fig. 8. (a) TDOS and different PDOS for the spin-polarized calculation for GaMn (model FM2), (b) Mn-*d* PDOS from the icosahedral sites, (c) Mn-*d* PDOS from the dodecahedral sites and (d) Ga PDOS.

different PDOS for this model. The majority (spin-up) direction is indicated by ↑ and the minority (spin-down) direction by ↓. As shown in Fig. 7a the DOS at the Fermi level for both spin-up and spin-down states are lower than that for the nonmagnetic case (around 20 states/eV/cell instead of 40 states/eV/cell for the paramagnetic calculation), which suggests some stability for the magnetically ordered structure. The PDOS of Mn 3*d* (dodeca) is opposite, with respect to the relative energies of spin-up and spin-down states to the PDOS of Mn 3*d* of the other Mn sites. The magnetic moment of each Ga atom is very close to zero, and remains nonmagnetic. Therefore, the DOS for the spin-up and spin-down states of Ga are very similar (Fig. 7d), although a small hybridization exists between Ga 4*p* and Mn 3*d* states.

4.3.2. *The FM2 model*

Fig. 8 illustrates the TDOS and different PDOS for this model. This second model is slightly less stable than FM1 by 0.24 eV. The TDOS for spin-up and spin-down states, shown in Fig. 8a, are very similar to each other, which is confirmed by the global total moment value of just 4.641 μ_B/cell. Indeed, the atomic moments on each Mn site are nearly equal, but among the icosahedral sites, six magnetic moments are antiparallel to the other six, which induces a small total magnetic moment for the icosahedra. The PDOS of each of these six sites are represented by solid and dashed curves in Fig. 8c. Figs. 8b and d, respectively, correspond to the PDOS Mn 3*d* (dodeca) and Ga, which are similar to what we observed for FM1 in Figs. 7b and d. However, in this case, the Fermi level falls on a peak of the DOS for the spin-up states as seen in Fig. 8a–c. From the point of view of electronic stability, even if this model is more stable than the paramagnetic one, the position of the Fermi level in the spin-up bonds could explain why FM1 remains more stable.

5. Discussion

Although the magnitudes of the local atomic magnetic moments of the two models are similar, the differences in signs at the various Mn sites are significant. These two different magnetic structures are shown in Fig. 9 with large black and white circles used to indicate relative spin orientations. Sakuma, working on the electronic structure of the ferromagnetic δ-GaMn phase, has found that Mn and Ga have a magnetic moment of 2.449 and $-0.088\,\mu_B$, respectively [10,11], which are consistent with the values we have found (Table 5). As a consequence of Mn 3*d*/Ga 4*p* hybridization, we observe a small magnetic moment at the Ga sites. However, slight differences exist among the different gallium atoms. In fact, the larger the number of manganese nearest neighbors, the greater the magnetic moment of the Ga atom. Indeed, in the GaMn structure, three independent Ga sites occur: one is surrounded by 12 Mn atoms (Ga1 icosahedral sites) whereas six Mn atoms and seven Ga atoms surround the two others. As a consequence of this local environment, Ga1 has a larger

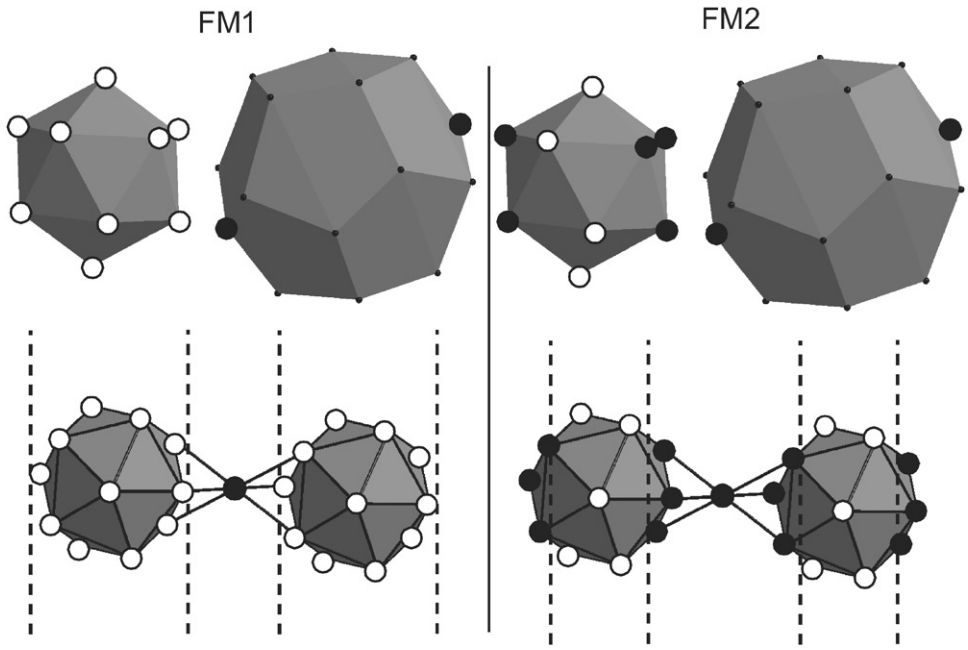

Fig. 9. Schematic representation of the localization of the different Mn atomic moments for both models FM1 and FM2. Large black and white circles represent the respective signs of the magnetic moments of the Mn atoms.

negative magnetization in comparison to the Ga3 and Ga6 sites (Table 5).

In the FM2 model a discussion of possible magnetic frustration is necessary since the Mn–Mn couplings in the icosahedra are AFM. Indeed, fixing the magnetic moment on two sites of a triangle where the coupling is AFM implies a frustration for the third site. In FM2 the moment at one atomic site is antiparallel to other two. However, by symmetry two faces of the icosahedral sites should possess three parallel moments and those two faces are neighboring the Mn sites of the dodecahedra. Nevertheless, magnetic frustration is a possibility, which could decrease the average magnetic moment of GaMn and could affect its magnetic behavior. A third model was tried with mostly AFM couplings along the c-axis from FM2 by changing the sign of the moment at the Mn atom of the dodecahedra. This model is unstable and the calculation converges back to FM2. Some experimental research, using molecular beams, has been made on different Mn clusters [29], and shows superparamagnetism of these clusters with local minima of μ_{atom} for the 13-atom icosahedron and the 19-atom double icosahedron (high coordinated "closed shell" species). This observation could suggest a preference for the FM2 model, for the solid-state example, although FM1 is calculated to have a lower energy within the TB-LMTO-ASA method.

In the GaMn structure, we can consider two different couplings: a J_1 coupling between Mn atoms within the icosahedra (Mn(ico)–Mn(ico)) and a J_2 coupling between the icosahedron and the bridging atom (Mn(ico)–Mn(dodeca)). To analyze these couplings separately and to understand the relative stability between the FM1 and FM2 models, two additional calculations have been performed: (1) replacing Mn2 by an empty sphere and (2) replacing Mn4 by an empty sphere. In (1), from the magnetic point of view, only the icosahedra are treated and they do not interact with each other. In (2) only the double tetrahedron is magnetically treated (Fig. 1c). These two cases are schematically represented below (the icosahedra are represented by circle).

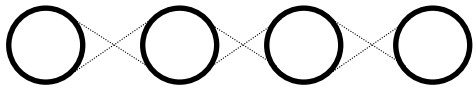

1

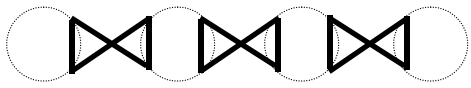

2

For both cases, calculations have been performed with the nonmagnetic model (PM), FM1 and FM2 models. In both, the PM model was the least stable and is our energy reference to compare the relative energy of the FM1 and FM2 models. In (1) the energy of FM1 and FM2 models are, respectively, −1.54 and −1.82 eV. These results are in good agreement with the molecular beams results [29]. In (2) the energy of FM1 and FM2 models are, respectively, −3.24 and −3.15 eV. In both cases, the model with antiferromagnetically coupled moments is more stable than the one with ferromagnetic coupling. The energy differences in case 2 are larger, doubled these in case 1, which suggests that the J_2 coupling is more important than the J_1 coupling. The

short Mn–Mn distances (2.576 Å) can be the reason for this strong interaction.

To summarize, the preference for the AFM coupling in the isolated icosahedra has been shown. However, the existence of the Mn(dodeca) sites, which couple the icosahedra along the *c*-axis modifies the different couplings. The J_2 coupling between the icosahedra and Mn(dodeca) is stronger than the J_1 coupling within icosahedra and influences the antiferromagnetism between those sites. These results explain the relative stability of FM1 versus FM2.

6. Concluding remarks

Using X-ray diffraction, the GaMn structure has been solved. The structure is close to the Al_8Cr_5 structure type proposed, but a centrosymmetric space group is preferred. The complexity of the binary phase diagram makes the synthesis of a pure sample of GaMn very difficult, which is one reason why no experimental magnetic data are yet available on GaMn. However, due to the relationship of this structure to quasicrystals, electronic structure calculations have been carried out based upon hypothetical magnetic structures. Only two different magnetic models converged (FM1 and FM2). We are now pursuing experiments to increase the yield of GaMn and to prepare large single crystals.

Acknowledgments

The Ames Laboratory is operated for the US Department of Energy by Iowa State University under contract No. W-7405-ENG-82. This work was supported by the Office of Basic Energy Sciences, Materials Sciences Division of the US Department of Energy. Also, a part of this work was supported by the NSF DMR 99-81766. The authors are grateful to Warren Straszheim of the Materials Analysis Research Laboratory of Iowa State University for running energy-dispersive X-ray spectroscopy measurements on our samples.

References

[1] M. Hasegawa, I. Tsuboya, Rev. Electr. Commun. Lab. 16 (7) (1960) 605.
[2] K.H.J. Buschow, P.G. van Engen, R. Jongebreur, J. Magn. Magn. Mater. 38 (1983) 1.
[3] K. Schubert, T.R. Anantharaman, H.O.K. Ata, H.G. Meissner, M. Pötzschke, W. Rossteutscher, E. Stolz, Naturwissenschaften 47 (1960) 512.
[4] K. Girgis, H. Schulz, Naturwissenschaften 58 (2) (1960) 95.
[5] H.G. Meissner, K. Schubert, Z. Metallkd. 56 (1965) 523.
[6] E. Kren, G. Kadar, Solid. State. Commun. 8 (1970) 1653.
[7] H. Niida, T. Hori, Y. Nakagawa, J. Phys. IV C8 49 (12) (1988) 173.
[8] E. Fawcett, H.L. Alberts, V.Yu. Galkin, D.R. Noakes, J.V. Yakhmi, Rev. Mod. Phys. 66 (1994) 25.
[9] M. Tanaka, J.P. Harbison, J. De Boeck, T. Sands, B. Philips, T.L. Cheeks, V.G. Keramidas, Appl. Phys. Lett. 62 (1993) 1565.
[10] A. Sakuma, J. Magn. Magn. Mater. 187 (1998) 105.
[11] Z. Yang, J. Li, D.-S. Wang, K. Zhang, X. Xie, J. Magn. Magn. Mater. 182 (1998) 369.
[12] E. Wachtel, K.J. Nier, Z. Metallkd. 56 (1965) 779.
[13] Stoe X-Shape Program, Crystal Optimization for Numerical Absorption Correction; Stoe & Cie Gmbh, Darmstadt, Germany, 1996.
[14] V. Petricek, M. Dusek (2000). The crystallographic computing system JANA2000. Institute of Physics, Praha, Czech Republic.
[15] M.A. Taylor, Acta Crystallogr. 14 (1961) 84.
[16] K. Hiraga, M. Kaneko, Y. Matsuo, S. Hashimoto, Philos. Mag. B 67 (1993) 193.
[17] N.C. Shi, X.Z. Li, Z.S. Ma, K.H. Kuo, Acta Crystallogr. B 50 (1994) 22.
[18] K. Robinson, Acta Crystallogr. 7 (1954) 494.
[19] M. Boström, S. Hovmöller, J. Alloys Compd 314 (2001) 154.
[20] M. Boström, S. Hovmöller, Acta Crystallogr. B 57 (2001) 646.
[21] (a) O.K. Andersen, Phys. Rev. B 12 (1975) 3060.
(b) O.K. Andersen, O. Jepsen, Phys. Rev. Lett 53 (1984) 2571.
(c) O.K. Andersen, O. Jepsen, D. Glötzel, in: F. Bassani, F. Fumi, M.P. Tosi (Eds.), Highlights of Condensed-Matter Theory, North-Holland, New York, 1985.
(d) W.R.L. Lambrecht, O.K. Andersen, Phys. Rev. B 34 (1986) 2439.
[22] U. von Barth, L. Hedin, J. Phys. C 5 (1972) 1629.
[23] D.D. Koelling, B.N. Harmon, J. Phys. C 10 (1977) 3107.
[24] O. Jepsen, O.K. Andersen, Z. Phys. B 97 (1995) 35.
[25] P.E. Blöchl, O. Jepsen, O.K. Andersen, Phys. Rev. B 49 (1994) 16223.
[26] T. Hughbanks, R. Hoffmann, J. Am. Chem. Soc. 105 (1983) 3528.
[27] R. Dronskowski, G.A. Landrum, Angew. Chem. Int. Ed. 39 (2000) 1560.
[28] E.C. Stoner, Proc. R. Soc. London 165 (1938) 372.
[29] M.B. Knickelbein, Phys. Rev. Lett. 86 (23) (2001) 5255.